PNAS RESEARCH ARTICLE | MEDICAL SCIENCES

Blockage of MLKL prevents myelin damage in experimental diabetic neuropathy

Jia Guo[a,b,1], Zehui Guo[b,1], Yanju Huang[c], Suchen Ma[c], Bo Yan[a,b], Chenjie Pan[a,b], Zhaodi Jiang[a,b], Fengchao Wang[a,b], Zhiyuan Zhang[a,b], Yuwei Da[d], Xiaodong Wang[a,b,2], and Zhengxin Ying[c,2]

Edited by Vishva Dixit, Genentech, San Francisco, CA; received November 27, 2021; accepted February 14, 2022

Demyelination is a pathological feature of diabetic neuropathy, a common and painful complication of diabetes, yet the mechanisms underlying diabetes-induced demyelination remain unclear. Here, we show that targeting mixed lineage kinase domain–like protein (MLKL), a protein critical in necroptosis, using Schwann cell–specific genetic knockout, S441A single–amino acid knockin mutation, or pharmacological inhibition all blocked myelin sheath decompaction and prevented the decrease of nerve conduction velocity in streptozotocin-induced diabetic mice. The decompaction of the myelin sheaths of sural nerves was observed in biopsy samples from diabetic patients, and the MLKL-mediated myelin breakdown was activated in human diabetic neuropathy patients. Our study establishes a direct myelin degradation–related role for MLKL in diabetic neuropathy and defines MLKL as a druggable target for developing agents to prevent or treat diabetic neuropathy.

diabetic neuropathy | MLKL | myelin

Significance

Diabetic neuropathy is a commonly occurring complication of diabetes that affects hundreds of millions of patients worldwide. Patients suffering from diabetic neuropathy experience abnormal sensations and have damage in their peripheral nerve axons as well as myelin, a tightly packed Schwann cell sheath that wraps around axons to provide insulation and increases electrical conductivity along the nerve fibers. The molecular events underlying myelin damage in diabetic neuropathy are largely unknown, and there is no efficacious treatment for the disease. The current study, using a diabetic mouse model and human patient nerve samples, uncovered a molecular mechanism underlying myelin sheath damage in diabetic neuropathy and provides a potential treatment strategy for the disease.

Diabetic neuropathy is by far the most prevalent complication of diabetes mellitus, a major human disease estimated to affect 536.6 million people worldwide and to cost $966 billion in health expenditures globally in 2021 (1). Diabetes-induced damage of the peripheral nervous system results in symptoms including pain, tingling, prickling sensations, and numbness in the feet and hands. Despite decades of research, there are no treatments for diabetic neuropathy other than glycemic control and lifestyle modifications (2).

The progression of diabetic neuropathy involves distal-to-proximal damage along the sensory nerve in the periphery, causing axon degeneration and demyelination. Among the known contributing factors to diabetic neuropathy are hyperglycemia, hyperlipidemia, microcirculatory dysfunction, and impaired insulin signaling (3). With prolonged excess glucose and lipid loads, oxidative phosphorylation fails, causing elevation of reactive oxygen species (ROS) and decreased ATP production, which subsequently leads to oxidative damage and mitochondrial failure in Schwann cells and axons (4). Increased glucose levels also result in the redirection of glucose into polyol and hexosamine metabolism, which can compound the deleterious impacts of increased ROS and inflammation (5, 6). Furthermore, increased glucose also promotes advanced glycation end products of structural and functional proteins that result in alteration (or loss) of protein function, and ROS are known to contribute to impaired epineural blood vessels, resulting in ischemic damage to axons and Schwann cells (7, 8).

Despite these findings, whether axonal loss or demyelination is the primary lesion of diabetic neuropathy remains debated (9). Diabetic neuropathy is generally considered to be an axonal neuropathy rather than a demyelinating disease per se. However, in myelinated fibers, the myelin sheath covers more than 99% of the axonal area; this sheath is a blood–nerve barrier that physically blocks exchange between the extracellular milieu and the underlying axonal compartment, thereby preventing axons from accessing glucose and other metabolites (10). There are reports from human diabetic neuropathy patients showing segmental demyelination without prominent axonal degeneration (9), suggesting that demyelination could happen without axonal damage. Therefore, understanding the demyelination process during diabetic neuropathy should facilitate the development of mechanism-based therapies for preventing diabetes-associated complications or treating ongoing myelin degradation.

Demyelination is a process known to be executed coordinately by immune cells and myelin-forming cells, including Schwann cells. In the peripheral nervous system, in response to nerve injury, the protein mixed lineage kinase domain–like protein (MLKL), which is known to function in a form of regulated necrotic cell death known as necroptosis (11) as well as demyelination (12), is induced in Schwann cells. Upon activating phosphorylation of its serine 441 site (mouse origin), MLKL in Schwann

Author contributions: J.G., Z.G., C.P., X.W., and Z.Y. designed research; J.G., Z.G., Y.H., S.M., C.P., and Z.J. performed research; B.Y., F.W., Z.Z., and Y.D. contributed new reagents/analytic tools; J.G., Z.G., Y.H., S.M., Z.J., Y.D., X.W., and Z.Y. analyzed data; and X.W. and Z.Y. wrote the paper.

The authors declare no competing interest.

This article is a PNAS Direct Submission.

Copyright © 2022 the Author(s). Published by PNAS. This article is distributed under Creative Commons Attribution-NonCommercial-NoDerivatives License 4.0 (CC BY-NC-ND).

See online for related content such as Commentaries.

[1]J.G. and Z.G. contributed equally to this work.

[2]To whom correspondence may be addressed. Email: wangxiaodong@nibs.ac.cn or yingzhengxin@cau.edu.cn.

This article contains supporting information online at http://www.pnas.org/lookup/suppl/doi:10.1073/pnas.2121552119/-/DCSupplemental.

Published March 28, 2022.

Downloaded from https://www.pnas.org by 217.105.28.28 on April 14, 2025 from IP address 217.105.28.28.

cells changes from a loosely membrane-associated protein to an integral membrane protein of the myelin sheath and functions to break down the tightly packed myelin sheaths (12). Notably, this serine 441 phosphorylation of MLKL is distinct from the phosphorylation modifications that occur during necroptosis, which are known to be mediated by RIP3 kinase (12, 13). RIP3 phosphorylates the serine 345/347 and threonine 349 sites, thereby enabling MLKL to oligomerize and insert onto the plasma membrane to disrupt the membrane integrity of cells undergoing necroptosis (11, 14).

Here, seeking to study the role of MLKL in the demyelination process in diabetic neuropathy, we used a streptozotocin (STZ)-induced diabetic mouse model in wild-type (WT) and several strains of genetically modified mice bearing changes in their *Mlkl* gene. We found that MLKL is inducibly expressed in Schwann cells in the sural nerves of diabetic mice and showed that genetically blocking the demyelination activity of MLKL via knockout or S441A knockin mitigated demyelination and diabetes-associated decreases in nerve conduction velocity (NCV). Moreover, using an MLKL-specific inhibitor (TC013249), we showed that pharmacological inhibition of MLKL slowed down myelin sheath damage and prevented the decrease of NCV. Finally, we demonstrated that MLKL-mediated demyelination occurs in patients with diabetic neuropathy.

Results

STZ-Induced Diabetes Results in Myelin Decompaction and MLKL Expression in the Sural Nerves of Mice. To study demyelination in diabetic neuropathy, we used a single-dose STZ injection to induce diabetes in mice. One and 2 wk after STZ injection, blood glucose monitoring revealed that the blood glucose levels of the treated mice started to rise by 1 wk after STZ treatment, reaching a mean of 29.7 mmol/L at 2 wk (*SI Appendix*, Fig. S1*A*). Mice with nonfasting blood glucose exceeding 25 mmol/L were then used for the following experiments.

Next, we used transmission electron microscopy (TEM) to examine the ultrastructures of myelin sheaths from the proximal, middle, and distal (sural nerve) segments of their sciatic nerves at 24 wk post-STZ injection. Compared to the tightly packed myelin membrane of intact nerves from the vehicle-injected control mice, the sural nerve myelin sheathes of the diabetic mice were clearly undergoing decompaction, exhibiting electron-sparse patches between the myelin sheaths (Fig. 1*A*). Moreover, the pattern of decompaction demonstrated a trend of proximal-to-distal increase, as the myelin sheaths in the distal region of the nerve became more severely decompacted than the proximal region (Fig. 1*A*).

To test if the observed demyelination in the sural nerve of diabetic mice is MLKL mediated, we looked for the expression of MLKL protein in the sural and sciatic nerves and found that MLKL in these regions in diabetic mice were detectable at 4 wk after STZ injection, with the strongest signal found in the sural nerves (Fig. 1*B*). There was no MLKL present in the sural and sciatic nerve in the vehicle (saline)-injected mice (Fig. 1*B*). Immunohistochemistry staining revealed extensive colocalization of MLKL protein and myelin basic protein (MBP; a myelin sheath marker) in the sural nerves of diabetic mice (Fig. 1*C*), further supporting a possible role for MLKL in the observed decompaction of myelin.

***Mlkl* Deficiency Prevents Myelin Decompaction and Decreases in NCV in Diabetic Mice.** To further study the role of MLKL in myelin decompaction in diabetic neuropathy, we first examined

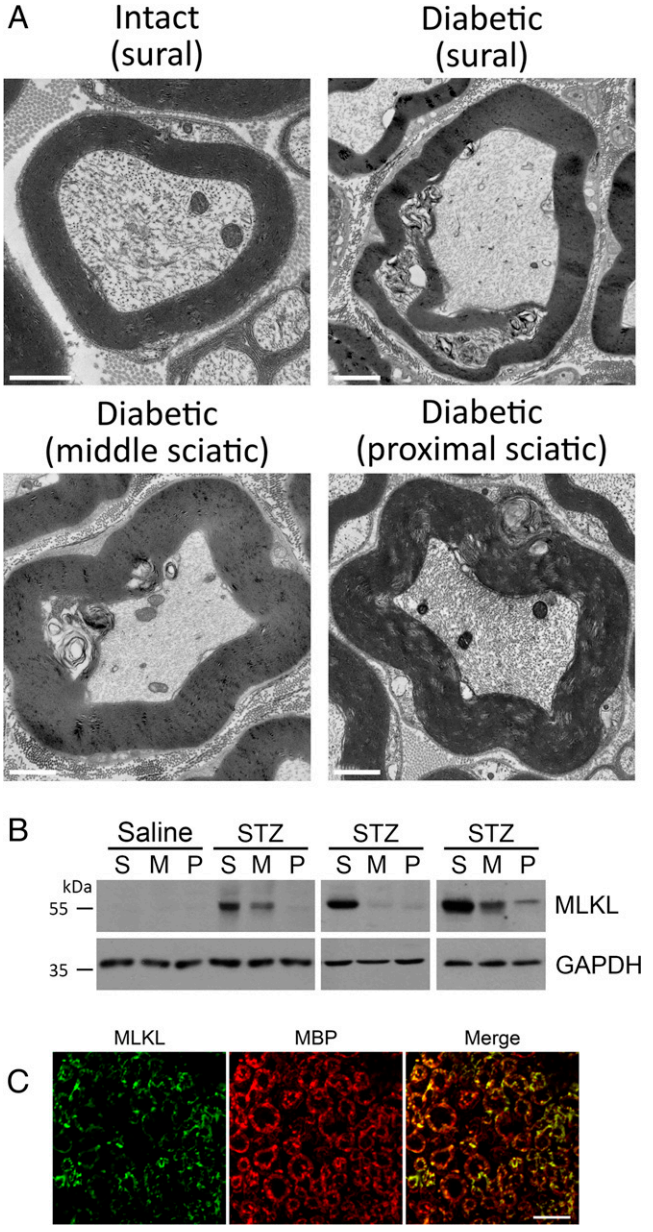

Fig. 1. STZ induces MLKL expression and causes sural nerve demyelination. (*A*) Twenty-four weeks after STZ injection, the ultrastructure of myelin in sural nerves was visualized by TEM. Whereas control mice had tightly packed myelin sheaths around their sural nerve, in STZ-treated mice, these myelin sheaths exhibited strong distal-to-proximal decompaction. (Scale bars, 1 μm.) (*B*) Immunoblotting with an antibody against MLKL in the distal (sural nerve [S]), middle (M), and proximal (P) segments of sciatic nerves in control and STZ-induced diabetic models; MLKL levels increased in sural nerves in diabetic mice. GAPDH was used as a loading control. (*C*) Representative immunofluorescence staining for MLKL (green) and the myelin sheath marker protein MBP (red) as well as their merged images on sural nerve sections from diabetic mice 8 wk after STZ injection. Note the high levels of colocalization between MLKL and MBP. (Scale bar, 10 μm.)

whether STZ can induce diabetes in *Mlkl*-deficient mutant mice. In $Mlkl^{-/-}$ mice, no MLKL was detected in the sural nerve section or protein sample after STZ injection, confirming *Mlkl* knockout (*SI Appendix*, Fig. S1 *B* and *C*). We then performed a glucose tolerance test on WT and $Mlkl^{-/-}$ diabetic mice and found that $Mlkl^{-/-}$ mice had similar blood glucose responses as the WT mice (*SI Appendix*, Fig. S1*D*). Moreover, upon STZ injection, the blood glucose levels in $Mlkl^{-/-}$ mice increased similarly to that of WT mice (*SI Appendix*, Fig. S1*E*). These results collectively excluded any obvious role for MLKL

Downloaded from https://www.pnas.org by 217.105.28.28 on April 14, 2025 from IP address 217.105.28.28.

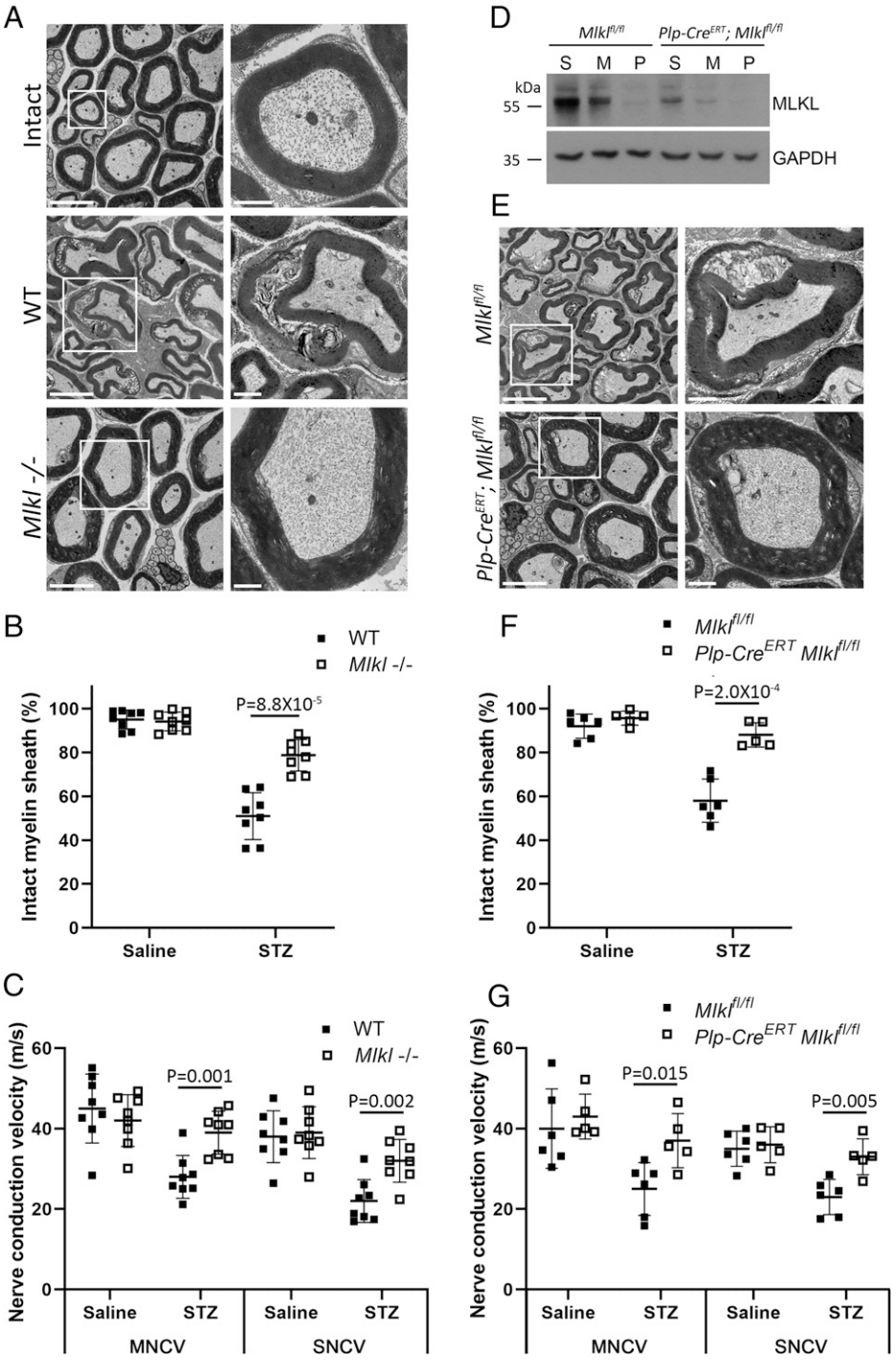

Fig. 2. Whole body or Schwann cell–specific *Mlkl* deficiency prevents myelin decompaction and NCV decrease in diabetic mice. (*A*) Representative TEM images of the ultrastructures of the myelin sheaths of intact sural nerves and sural nerves from WT ($n = 8$) and $Mlkl^{-/-}$ diabetic mice ($n = 8$). *Left*, low magnification. (Scale bars, 5 μm.) *Right*, high magnification of the boxed regions on the left. (Scale bars, 1 μm.) Note that the $Mlkl^{-/-}$ mice exhibited significantly less severe myelin sheath decompaction than WT mice. (*B*) Quantification of intact myelin rings in WT and $Mlkl^{-/-}$ diabetic mice ($n = 150$ myelin rings for each group). (*C*) At 24 wk post-STZ or control saline injection, the MNCVs and SNCVs of WT and $Mlkl^{-/-}$ mice were measured. $MLKL^{-/-}$ diabetic mice had significantly faster NCVs. (*D*) Immunoblotting of MLKL levels in $Plp\text{-}Cre^{ERT}$; $Mlkl^{fl/fl}$ and $Mlkl^{fl/fl}$ diabetic mice to assess Schwann cell–specific MLKL knockout; the distal (sural nerve), middle, and proximal segments of sciatic nerves were analyzed. MLKL levels were significantly lower in $Plp\text{-}Cre^{ERT}$; $Mlkl^{fl/fl}$ mice. GAPDH was used as a loading control. (*E*) Representative TEM images of the ultrastructures of the myelin sheaths of sural nerves from $Plp\text{-}Cre^{ERT}$; $Mlkl^{fl/fl}$ ($n = 6$) and $Mlkl^{fl/fl}$ ($n = 5$) diabetic mice. *Left*, low magnification. (Scale bars, 5 μm.) *Right*, high magnification of the boxed regions on the left. (Scale bars, 1 μm.) (*F*) Quantification of *E* shows that Schwann cell–specific knockout of MLKL significantly blocked myelin sheath decompaction ($n = 150$ myelin rings for each group). (*G*) An NCV test showed that diabetic mice with Schwann cell–specific knockout of MLKL had significantly faster NCVs. Data are represented as mean ± SD.

in glucose homeostasis or the metabolic disorder diabetes per se.

We next analyzed the morphology of the myelin sheath in sural nerves from WT and $Mlkl^{-/-}$ diabetic mice. Despite both genotypes having similar blood glucose levels, the $Mlkl^{-/-}$ mice had conspicuously better preserved myelin structures after diabetic induction (Fig. 2 *A* and *B*). At 24 wk post-STZ injection, the myelin sheaths of the WT mice exhibited severe pathological changes, including extensive lamina decompaction and widespread vacuolization (Fig. 2 *A*, *Middle*). In contrast, the

Downloaded from https://www.pnas.org by 217.105.28.28 on April 14, 2025 from IP address 217.105.28.28.

myelin sheaths of the *Mlkl*$^{-/-}$ mice appeared similar to the nondiabetic mice, showing only spotty vacuolization within the packed myelin sheaths (Fig. 2 *A*, *Bottom*). These results indicate that MLKL protein has a role in driving demyelination of sural nerves in diabetic mice.

Because myelin damage decreases NCV, and diabetic animals are known to have slower NCVs, we then examined NCV in WT and *Mlkl*$^{-/-}$ diabetic mice. Twenty-four weeks after STZ injection, diabetic WT mice showed significantly decreased NCVs compared to non–STZ-induced control mice (Fig. 2*C*), revealing the anticipated diabetes-associated compromised nerve function. Strikingly, the NCVs of the *Mlkl*$^{-/-}$ diabetic mice were much faster than the WT diabetic mice (Fig. 2*C*).

To confirm that the observed prevention in demyelination and decreased NCV in *Mlkl*$^{-/-}$ mice indeed resulted from the lack of MLKL expression in Schwann cells, we used STZ injection to induce diabetes in Schwann cell–specific *Mlkl*-knockout mice, generated by crossing *Mlkl* flox/flox mice with transgenic mice harboring a locus for the tamoxifen-inducible Plp1 (proteolipid protein 1) promoter-driven expression of Cre (Plp1-Cre/ERT) and administrating tamoxifen intraperitoneally every other day for 12 d. As shown in the immunoblots in Fig. 2*D*, the Plp1-driven Cre expression–mediated Schwann cell–specific *Mlkl* knockout significantly reduced the induction of MLKL in sural and sciatic nerves in these STZ-induced diabetic mice. Furthermore, TEM analysis revealed better-preserved myelin sheath ultrastructures in these Schwann cell conditional *Mlkl*-knockout mice than in WT mice (Fig. 2 *E* and *F*), and the decreased NCVs of the diabetic conditional knockout mice were less severe than those observed in the WT diabetic mice (Fig. 2*G*). These results demonstrate that the myelin decompaction and decreased NCVs in diabetic mice require Schwann cell–specific expression of MLKL.

Replacement of the WT *Mlkl* Gene with a Serine 441–to-Alanine Mutant Prevented Myelin Decompaction and NCV Decrease in Diabetic Mice. Our previous study showed that serine 441 (S441) phosphorylation of MLKL during sciatic nerve injury activates MLKL in Schwann cells to execute myelin breakdown (12). To test whether the S441 residue is also required for MLKL-mediated myelin breakdown in diabetic mice, we generated S441A point mutation knockin mice (*SI Appendix*, Fig. S2 *A* and *B*). In these mice, the axotomy-induced demyelination in sciatic nerves was significantly delayed to a level similar to that observed in *Mlkl*-knockout mice (*SI Appendix*, Fig. S2 *C* and *D*). However, the nerve injury–induced MLKL expression levels did not change between the WT and S441A-knockin mice (*SI Appendix*, Fig. S2*E*), indicating that the delayed demyelination was not caused by the lack of MLKL expression and that the serine 441 is indeed critical for MLKL activation during axotomy-induced demyelination in sciatic nerves. Additionally, and consistent with our previous finding that the activating phosphorylation of the demyelination function of MLKL is different and independent of the ones essential for necroptosis, we found that bone marrow–derived macrophages (BMDMs) isolated from S441A mice still respond to necroptotic stimuli, similar to WT BMDMs, whereas BMDMs from *Mlkl*-knockout mice were completely resistant to necroptotic stimuli (*SI Appendix*, Fig. S2*F*).

Phosphorylation of MLKL at S441 is required for insertion of MLKL into the lipid bilayer of myelin sheaths, and S441A-mutant MLKL fails to do so upon sciatic nerve injury (12). To test the lipid bilayer insertion of MLKL in the sural nerve of diabetic mice, we first used STZ to induce diabetes in WT and MLKL S441A–knockin mice and then used alkaline buffer wash followed by differential centrifugation to isolate MLKL specifically inserted in the membrane (12). We found that WT MLKL behaved as an integral membrane protein and localized in the alkaline wash–resistant fraction (Fig. 3*A*, P150 fraction), whereas S441A-mutant MLKL was located in the peripheral membrane fraction that was washed off the membrane by alkaline buffer (Fig. 3*A*, S150 fraction). Moreover, the decompaction of myelin sheaths (Fig. 3 *B* and *C*) and the decreased NCVs (Fig. 3*D*) were both mitigated in MLKL S441A diabetic mice. These results confirmed that the S441 residue of MLKL is required for MLKL's role in the breakdown of the myelin sheaths of injured and diabetic nerves.

Treatment of Diabetic Mice with an MLKL Inhibitor Prevents Myelin Decompaction and Decreases NCV in Diabetic Mice. Since *Mlkl* deficiency slows down myelin breakdown and prevents decreased NCVs in diabetic mice, we investigated the use of an MLKL inhibitor as a possible treatment for the demyelination that occurs in diabetic neuropathy. Such inhibitors have been developed against human MLKL (hMLKL) by taking advantage of a binding pocket within its N terminus membrane-disrupting helix bundle, near where a hMLKL-specific cysteine 86 can be covalently targeted to achieve nanomolar efficacy in cellular antinecroptosis assays (15). Since a compound like TC013249 used here was specifically developed to target hMLKL, we first generated an hMLKL-knockin mouse (hMLKL-KI) that expressed hMLKL under the control of the endogenous Mlkl promoter (*SI Appendix*, Fig. S3*A*). hMLKL-KI mice express hMLKL but not mouse MLKL (*SI Appendix*, Fig. S3*D*). The hMLKL-KI and WT mice showed similar MLKL expression levels and degree of myelin breakdown in their sciatic nerves 3 d after axotomy (*SI Appendix*, Fig. S3 *B*–*D*). However, consistent with the previous finding in cultured cell lines that hMLKL cannot substitute mouse MLKL for necroptosis in mouse cells (16–18), we found that BMDMs isolated from hMLKL-KI mice did not respond to necroptotic stimuli (*SI Appendix*, Fig. S3*E*) nor did hMLKL oligomerize upon such stimulation (*SI Appendix*, Fig. S3*F*). These results establish that when mouse MLKL is substituted by hMLKL, hMLKL can only execute demyelination but not necroptosis, thus making hMLKL-KI mice a useful tool to study nonnecroptotic functions of MLKL.

To confirm the efficacy of the MLKL inhibitory compound TC013249, we first examined its ability to prevent necroptosis in the human colon cancer cell line HT-29. We found that TC013249 dose dependently blocked the death of HT-29 cells at single-digit nanomolar concentrations when the cells were exposed to necroptotic stimuli (*SI Appendix*, Fig. S3*G*). We subsequently tested TC013249 in hMLKL-KI mice that have undergone axotomy procedures on their sciatic nerves and found that treatment of TC013249 (intraperitoneal injection) significantly slowed down axotomy-induced demyelination (*SI Appendix*, Fig. S3 *H* and *I*).

Since STZ-induced diabetic neuropathy is a chronic disease that requires continuous treatment with MLKL inhibitor, we intraperitoneally implanted osmotic pumps to deliver TC013249 or vehicle to hMLKL-KI and WT mice for an extended period. After the implantation of osmotic pumps for 7 and 14 d, the plasma concentration of TC013249 reached 2.8 ± 0.3 nM and 3.3 ± 0.5 nM, sufficient, in theory, to block a significant portion of MLKL activity. The TC013249 treatment did not alter the expected STZ model–induced increase

Downloaded from https://www.pnas.org by 217.105.28.28 on April 14, 2025 from IP address 217.105.28.28.

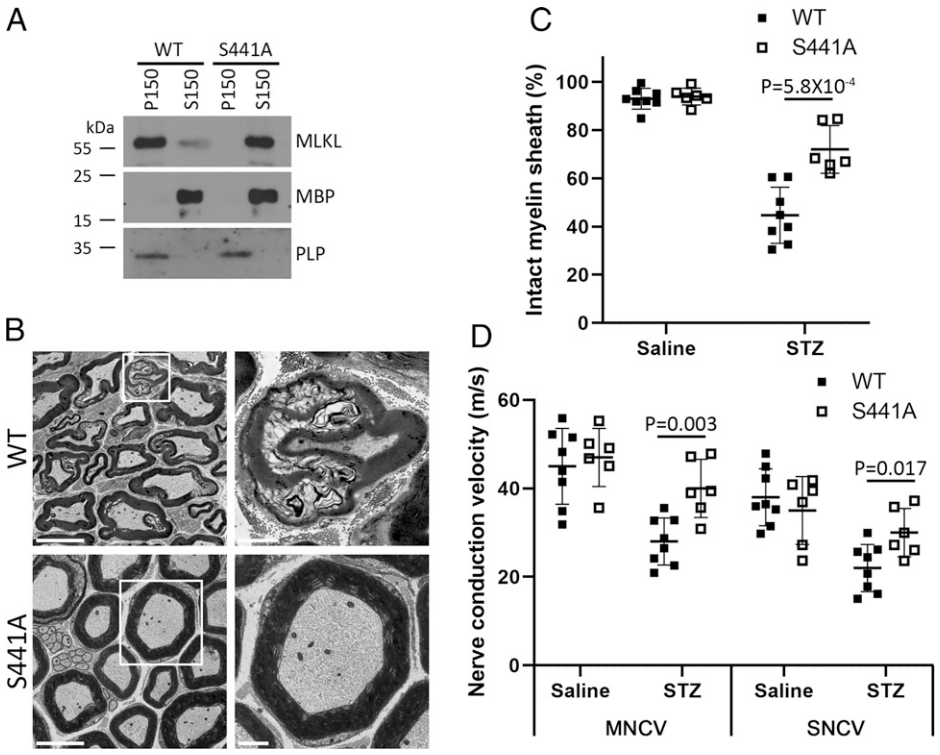

Fig. 3. *Mlkl* S441A–knockin mice are resistant to diabetes-induced myelin decompaction and NCV decrease. (*A*) Differential centrifugation of extracts from sural nerves in WT and S441A-knockin mice showed that WT MLKL was inserted into the lipid bilayer of the myelin sheath (in the same fraction as the PLP marker), but $MLKL^{S441A}$ was only loosely associated with the myelin sheath (in the same fraction as MBP). (*B*) Representative TEM images of the ultrastructures of the myelin sheaths of sural nerves from WT (n = 8) and S441A-knockin (n = 6) diabetic mice. *Left*, low magnification. (Scale bars, 5 μm.) *Right*, high magnification of the boxed regions on the left. (Scale bars, 1 μm.) (*C*) Quantification of *B* shows that the S441A mutation of MLKL significantly blocked myelin sheath decompaction (n = 150 myelin rings for each group). (*D*) An NCV test indicated that S441A MLKL-knockin diabetic mice had significantly faster NCVs. Data are represented as mean ± SD.

in blood glucose levels (*SI Appendix*, Fig. S3*J*) but blocked the myelin lipid bilayer insertion of hMLKL (Fig. 4*A*). This result thus indicated that the continuous pumping of TC013249 had reached a sufficient concentration in mouse sciatic nerves to block hMLKL activity. Consequently, treatment with TC013249 significantly mitigated both myelin sheath decompaction and decreased motor NCVs (MNCVs) in diabetic mice (Fig. 4 *B*–*D*). However, treatment of TC013249 had no effect in blocking myelin sheath decompaction in WT mice (*SI Appendix*, Fig. S3 *K* and *L*), confirming the specificity of TC013249 in targeting hMLKL. These results highlight MLKL as an attractive potential therapeutic target for developing treatments for diabetic neuropathy.

MLKL Activation Occurs in the Myelin Sheath of Patients with Diabetic Neuropathy. We next examined whether MLKL is also activated in patients with diabetic neuropathy. We first checked the myelin structure in biopsy samples of the sural nerve from 3 diabetic neuropathy patients (male age 65, female age 49, and male age 38). Immunofluorescence staining for neurofilament and MBP showed that there are large axons without myelin wrapping, empty myelin sheath, and degenerated axons wrapping with uncompacted myelin existing in the same sural nerve section (Fig. 5*A*). This confirms that myelin breakdown can happen independent of axon damage in diabetic neuropathy. Under structured illumination microscopy, myelin decompaction also appears in sural nerves of diabetic patients (Fig. 5*B*). We next examined whether MLKL also accumulated in the myelin of patients with diabetic neuropathy by staining sural nerve sections from biopsy samples. Compared to the age- and sex- matched healthy individuals, those from patients with diabetic neuropathy had more prominent MLKL signals in the myelin sheath (Fig. 5*C* and *SI Appendix*, Fig. S4 *A* and *B*).

Discussion

There is increasing data supporting the fact that Schwann cells are more than just passive insulators for axons. During diabetes, nutrient starvation of Schwann cells and axons due to microvasculature collapse or glucose overload causes Schwann cells to transfer toxic lipid species to axons, eventually leading to axon degeneration (19). Thus, the protection of myelin and Schwann cells should also be addressed in the treatment of diabetic neuropathy. Considering the close interaction between axons and myelin and the fact that Schwann cells metabolically and neurotrophically support axons to maintain axon integrity and energy homeostasis, Schwann cell damage during diabetes can lead to damage and degeneration of the axon (20, 21).

Schwann cell–selective knockout of liver kinase B1 (LKB1), a serine–threonine kinase that regulates Schwann cell energy homeostasis, can cause the degeneration of both myelin and axons (22). In diabetes, pyruvate and lactate generation is insufficient for Schwann cells to survive normally and support axons (23), and the typical lactate supply from Schwann cells to axons is reduced, lowering axonal energy metabolism (24). Consequently, the prolonged lower levels of axonal ATP ultimately led to axonal degeneration (25). Schwann cells also regulate the cytoskeletal properties of axons, including promoting maturation of the axon cytoskeleton and regulation of axon trafficking (26). Clearly, such notable discoveries about the expanded metabolic and cellular structural–functional roles of Schwann cells

Downloaded from https://www.pnas.org by 217.105.28.28 on April 14, 2025 from IP address 217.105.28.28.

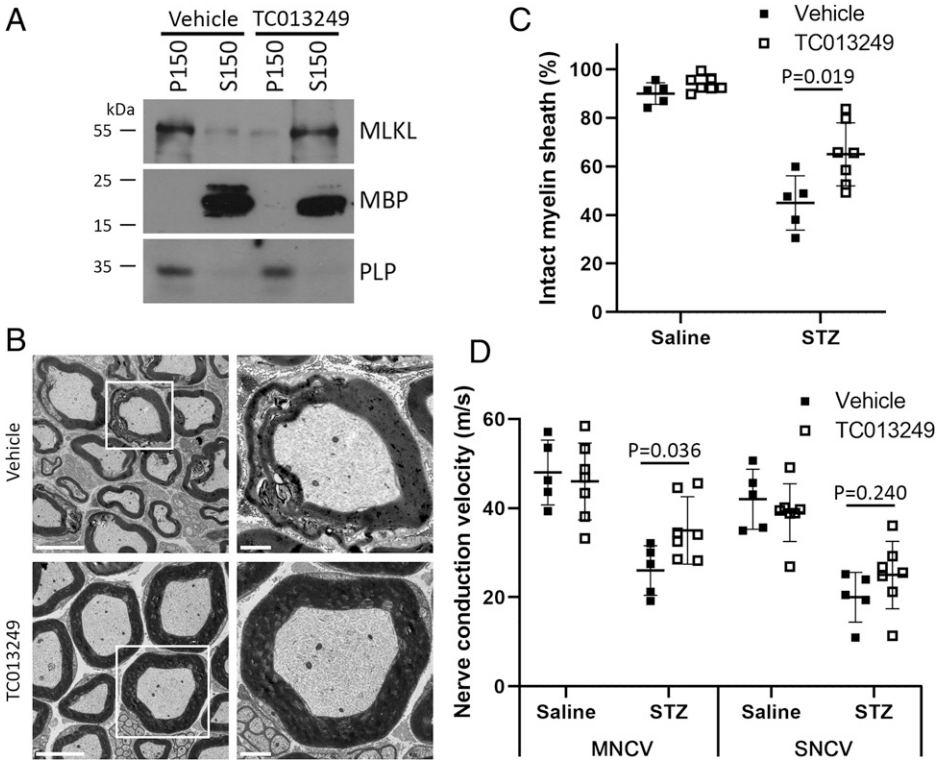

Fig. 4. An MLKL inhibitor blocks diabetes-induced myelin decompaction and NCV decrease. (*A*) Differential centrifugation of extracts from sural nerves in hMLKL-KI diabetic mice showed that MLKL was inserted into the lipid bilayer of the myelin sheath (in the same fraction as the PLP marker) but that MLKL was only loosely associated with the myelin sheath (in the same fraction as MBP) after TC013249 treatment. (*B*) Osmotic pumps, either containing vehicle or TC013249, were intraperitoneally implanted into mice ($n = 5$ for vehicle and $n = 7$ for TC013249) 4 wk post-STZ injection. Representative TEM images of the ultrastructures of the myelin sheaths of sural nerves from vehicle- and TC013249-treated hMLKL-KI diabetic mice. *Left*, low magnification. (Scale bars, 5 μm.) *Right*, high magnification of the boxed regions on the left. (Scale bars, 1 μm.) (*C*) Quantification of *B* shows that TC013249 treatment significantly blocked diabetes-induced myelin sheath decompaction ($n = 150$ myelin rings for each group). (*D*) An NCV test for vehicle- or TC013249- treated diabetic mice indicated that TC013249 treatment mitigated decreases in MNCV in diabetic mice. Data are represented as mean ± SD.

emphasize a substantial opportunity for targeting them to treat various forms of axon degeneration.

MLKL was first identified as a necroptosis executioner that disrupts membrane integrity to promote necroptotic cell death (11). Upon necroptotic stimuli, mouse MLKL is phosphorylated at its S345, S347 and T349 sites (or hMLKL at its S357 and T358 sites) by RIP3 kinase, after which it can form oligomers (14) and then translocate from the cytosol to the plasma membrane to disrupt plasma membrane integrity, thereby causing necrosis (27). In diabetic patients, no necroptotic MLKL phosphorylation was detected (*SI Appendix*, Fig. S4*C*). Later, MLKL was found to have an additional role in breakdown of the myelin sheathes in axotomy-induced demyelination, an activity that is triggered by phosphorylation of the S441 site by an unknown kinase that appears to be activated after nerve injury (12). The S441 phosphorylated MLKL then inserts into the lipid bilayer of the myelin sheath, presumably through binding to a myelin-enriched lipid known as sulfatide (12).

In the setting of diabetic neuropathy, MLKL seems to also have a role in the breakdown of the myelin sheaths of sciatic nerves (Fig. 2), thus making it a potential target for preventing demyelination in diabetic neuropathy. In diabetic mice, the pattern of myelin decompaction and MLKL expression both demonstrated a trend of proximal-to-distal increase. Whether this correlation is functionally relevant needs further investigation. In diabetic patients, both primary demyelination and demyelination secondary to axonal degeneration have been observed in the same nerve biopsy (Fig. 5*A*), and the expression of MLKL was detected (Fig. 5*C* and *SI Appendix*, Fig. S4*A*). Recent studies have shown that crosslinking fixative significantly compromises the ability of antibodies to recognize MLKL (28); thus, extra caution should be taken when processing formaldehyde-fixed biopsy samples.

Since demyelination can occur before any axon damage, protecting myelin should not only save this insulating material but also contribute to improved axonal integrity maintenance. In the present study, seeking to prevent demyelination in diabetic neuropathy, we used genetic and pharmacological approaches to block the activity of MLKL. Both knockout of *Mlkl* or loss-of-function knockin (S441A) of MLKL helped preserve the integrity of the myelin ultrastructure in diabetic mice. However, these genetic manipulations did not fully restore the ultrastructure or the function of myelin, suggesting the existence of other contributors to diabetes-induced demyelination. Pharmacologically, we used an hMLKL-specific inhibitor to block the activity of MLKL in mice expressing hMLKL instead of mouse MLKL. After MLKL inhibitor treatment, mice still developed diabetes (Fig. 4*A*), but the decompaction of the myelin sheath was largely blocked, thereby providing a proof of principle that MLKL is a valuable therapeutic target for the treatment of diabetic neuropathy.

Given that diabetic neuropathy is asymptomatic in some patients, this complication can be missed in diabetes diagnoses (2). Thus, developing diabetic neuropathy–specific biomarkers will help clinicians to identify actionable changes in the disease progressions of their patients, especially if such biomarkers are present in easily assayable sample materials. Thus, antibodies that recognize the human equivalent of S441 phosphorylation in MLKL could potentially be used to detect this biochemical marker for diabetic neuropathy.

Downloaded from https://www.pnas.org by 217.105.28.28 on April 14, 2025 from IP address 217.105.28.28.

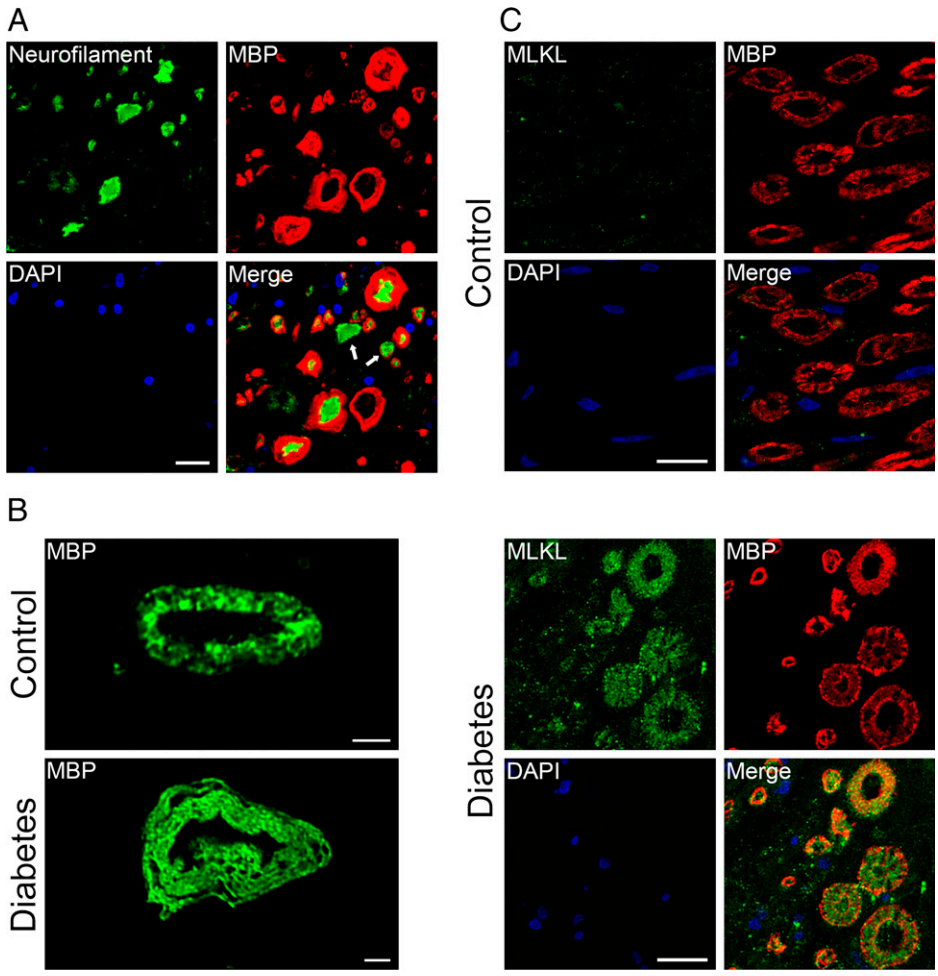

Fig. 5. MLKL is activated in the myelin sheath of diabetic neuropathy patients. (*A*) Sural nerve sections from human patients with diabetic neuropathy were analyzed by immunofluorescence staining with antibodies against neurofilament (green) and MBP (red), DAPI (diamidino-2-phenylindole) was used to visualize nuclei (blue). Note the existence of a large axon without myelin wrapping (arrows). (Scale bar, 10 μm.) (*B*) Structured illumination microscopy fluorescence image of MBP from patients with diabetic neuropathy and healthy individuals. (Scale bars, 1.5 μm.) (*C*) Sural nerve sections from human patients with diabetic neuropathy and healthy individuals were analyzed by immunofluorescence staining with antibodies against MLKL (green) and MBP (red). DAPI was used to visualize nuclei (blue). Note the colocalization of MLKL and MBP in patients with diabetic neuropathy. Data are representative of three patients with diabetic neuropathy and three people from the control group. (Scale bars, 10 μm.)

Materials and Methods

Reagents and Antibodies. All reagents were purchased from Sigma-Aldrich unless otherwise stated. The following antibodies were used: anti-MLKL (rabbit polyclonal, LSBio, LS-C334151, 1:100), anti-MLKL (rabbit monoclonal, Abcam, EPR17514, 1:1,000), anti-MLKL (rabbit monoclonal, Cell Signaling, 37705, 1:1,000), anti-MLKL (phospho S358, rabbit monoclonal, Abcam, ab187091, 1:250), anti-MBP (mouse monoclonal, Santa Cruz Biotechnology, sc-271524, 1:500), anti-PLP (rabbit monoclonal, Abcam, ab254363, 1:1,000), anti-neurofilament (rabbit monoclonal, Abcam, ab254348, 1:100), anti-GAPDH (mouse monoclonal, Abcam, ab8245, 1:2,000), goat anti-mouse IgG (horseradish peroxidase [HRP], Abcam, ab205719, 1:10,000), goat anti-rabbit IgG (HRP, Abcam, ab205718, 1:10,000), donkey anti-mouse (Alexa Fluor 488, Thermo Fisher, A-21202, 1:1,000), donkey anti-mouse (Alexa Fluor 555, Thermo Fisher, A-31570, 1:1,000), donkey anti-rabbit (Alexa Fluor 488, Thermo Fisher, A-21206, 1:1,000), and donkey anti-rabbit (Alexa Fluor 555, Thermo Fisher, A-31572, 1:1,000).

Ethics. All animal experiments were conducted following the Chinese Ministry of Health national guidelines for the housing and care of laboratory animals and were performed in accordance with institutional regulations after review and approval by the Institutional Animal Care and Use Committee of the National Institute of Biological Sciences, Beijing, and China Agricultural University. Sural nerve biopsies were collected and used under the ethical approval from China Agricultural University (CAUHR-2020013).

Animals. C57BL/6J mice were purchased from Vital River Laboratory Animal Technology Co. All animals used in this study were male and were housed in individually ventilated, specific pathogen–free cages with 12-h light/dark cycles with access to food and water ad libitum. The *Mlkl*-knockout mice were generated in previous studies (29). MLKL S441A point mutation–knockin and hMLKL-knockin (expressing hMLKL rather than murine Mlkl) mice were generated using the CRISPR-Cas9 system (*SI Appendix*, Figs. S2 *A* and *B* and S3*A*). Inducible Schwann cell–specific *Mlkl*-knockout mice were generated by crossing *Mlkl* flox/flox mice with transgenic mice harboring a locus for the tamoxifen-inducible Plp1 promoter–driven expression of Cre (Plp1-Cre/ERT). All genetically engineered mice are on a C57BL/6J background. To knockout *Mlkl* in Schwann cells of WT mice, 1 mg of tamoxifen per mouse was administrated intraperitoneally every other day for 12 d.

Diabetes Induction and Glucose Tolerance Test. STZ (dissolved in sodium citrate buffer, pH 4.5) was injected intraperitoneally at a dose of 160 mg/kg. Mice were provided with 10% sucrose water for 4 d following STZ injection (30). Blood glucose levels were measured by tail tip bleeding using a glucometer at 7 and 14 d after STZ injection. Mice with a nonfasting blood glucose level exceeding 25 mmol/L were used in this study. The glucose tolerance test was performed on 16-h fasted mice by intraperitoneal injection of 1 g/kg glucose. Blood glucose levels were measured before and at 30-, 60-, 90-, and 120-min intervals after the glucose injection.

Surgical Procedure. Deep-anesthetized mice (sodium pentobarbital, 200 mg/kg, intraperitoneal injection) were perfused via the aorta with cold phosphate-

Downloaded from https://www.pnas.org by 217.105.28.28 on April 14, 2025 from IP address 217.105.28.28.

buffered saline (PBS) and 4% paraformaldehyde for immunohistochemistry study or 2.5% glutaraldehyde and 2% paraformaldehyde for electron microscopy study. Osmatic pumps (ALZET, 1004) containing the hMLKL-specific inhibitor TC013249 were implanted intraperitoneally.

Immunohistochemistry and Immunoblotting. The sciatic nerves were post-fixed with 4% paraformaldehyde and cryoprotected with 20% sucrose. Nerves were embedded in a Tissue-Tek cryomold (Sakura), and 6-μm cryosections were cut and prepared on precoated slides. For human sural nerve sections, sections were deparaffinized, gradually rehydrated, treated with 10 mM citric acid buffer (pH 6.0), and heated in a microwave oven for antigen retrieval. Sections were blocked with SuperBlock blocking buffer (Thermo Scientific) for 1 h at room temperature. Tissue sections were then incubated with primary antibodies overnight at 4 °C and were then washed and incubated with secondary antibodies for 1 h at room temperature. Slides were covered with an antifade reagent (Prolong Diamond, Life Technologies).

Protein samples were electrophoresed on sodium dodecyl sulfate polyacrylamide gels and then transferred onto nitrocellulose membranes. Membranes were blocked with skim milk (5% in PBST [phosphate-buffered saline with 0.1% Triton-X-100]) at room temperature for 1 h. Membranes were then incubated with primary antibodies overnight at 4 °C, followed by incubation with secondary antibodies for 1 h at room temperature. Proteins were visualized based on chemiluminescence using Western Lightning Plus ECL reagent (PerkinElmer). GAPDH was used as a loading control.

Electron Microscopy. Sural nerves were postfixed with 2% paraformaldehyde and 2.5% glutaraldehyde, followed by secondary fixing with 1% OsO_4. Samples were then dehydrated through an ascending acetone series (15 to 100% in seven steps). The samples were then embedded in Epon 812 resin (Electron Microscopy Sciences) and sectioned to 70 nm. Sections were visualized using a Tecnai G2 Spirit electron microscope (FEI).

NCVs. NCVs were recorded at 24 wk post-STZ injection according to Stevens et al. (31). Body temperature was monitored with a rectal probe and maintained at 37 °C. MNCVs were obtained by measuring compound muscle action potentials using supramaximal stimulation distally at the ankle and proximally at the sciatic notch. Recordings were obtained from the first interosseous muscle. Sensory NCVs (SNCVs) were recorded behind the medial malleolus with a 0.5-ms square wave pulse using the smallest current to elicit a response, stimulating at the digital nerve of the second toe. NCV was the average of ten recordings.

Subcellular Fractionation. Tissues were homogenized in buffer A (20 mM HEPES, pH 7.4, 40 mM KCl, 1.5 mM $MgCl_2$, 1 mM ethylenediaminetetraacetic acid (EDTA), 1 mM ethylene glycol tetraacetic acid (EGTA), 250 mM sucrose) and centrifuged at 500 × *g* for 10 min, and the supernatant was harvested and recentrifuged at 20,000 × *g* for 10 min. The pellet containing the membrane fraction was washed twice and resuspended and homogenized in alkaline buffer (100 mM Na_2CO_3 and 500 mM NaCl) and centrifuged at 20,000 × *g* for 10 min. The supernatant was then centrifuged at 150,000 × *g* for 1 h. The supernatant containing the peripheral membrane proteins was designated as "S150." The pellet containing the integral membrane proteins was designated as "P150."

Cell Culture Cell Survival Assay. For culturing BMDMs, tibias were isolated and cut at both ends. The bones were then flushed with PBS, and bone marrow cells were passed through a 40-μm cell strainer; the collected cell suspensions were centrifuged at 1,000 × *g* for 5 min. The cell pellets were resuspended with Dulbecco's Modified Eagle's Medium containing 20% fetal bovine serum, 1% penicillin–streptomycin, and 30% (vol/vol) L929 conditioned medium and plated on cell culture plates. Cell viability was assayed by measuring ATP levels using a Cell Titer-Glo kit (Promega) according to the manufacturer's instructions.

Statistical Analyses. Differences between means were assessed by one-way ANOVA with a post hoc Tukey's analysis using Prism (GraphPad Software). Values are expressed as means ± SD, with differences considered significant at $P < 0.05$.

Data Availability. All study data are included in the article and/or *SI Appendix*.

ACKNOWLEDGMENTS. We thank Dr. John Hugh Snyder and Dr. Alex Wang for critically reading the manuscript. This work was supported by institutional grants from the Chinese Ministry of Science and Technology, the Beijing Municipal Science and Technology Commission, the National Natural Science Foundation of China (32100759), and the Chinese Universities Scientific Fund (2021RC013).

Author affiliations: [a]National Institute of Biological Sciences, Beijing 102206, China; [b]Tsinghua Institute of Multidisciplinary Biomedical Research, Tsinghua University, Beijing 102206, China; [c]State Key Laboratory of Agrobiotechnology, College of Biological Sciences, China Agricultural University, Beijing 100193, China; and [d]Xuanwu Hospital, Capital Medical University, Beijing 100053, China

1. International Diabetes Federation, *IDF Diabetes Atlas* (IDF, ed. 10, 2021). https://diabetesatlas.org/atlas/tenth-edition/. Accessed 9 January 2022.
2. R. Pop-Busui *et al.*, Diabetic neuropathy: A position statement by the American Diabetes Association. *Diabetes Care* **40**, 136–154 (2017).
3. E. L. Feldman *et al.*, Diabetic neuropathy. *Nat. Rev. Dis. Primers* **5**, 41 (2019).
4. P. Fernyhough, Mitochondrial dysfunction in diabetic neuropathy: A series of unfortunate metabolic events. *Curr. Diab. Rep.* **15**, 89 (2015).
5. X. L. Du *et al.*, Hyperglycemia-induced mitochondrial superoxide overproduction activates the hexosamine pathway and induces plasminogen activator inhibitor-1 expression by increasing Sp1 glycosylation. *Proc. Natl. Acad. Sci. U.S.A.* **97**, 12222–12226 (2000).
6. P. J. Oates, Aldose reductase, still a compelling target for diabetic neuropathy. *Curr. Drug Targets* **9**, 14–36 (2008).
7. D. W. Zochodne, Mechanisms of diabetic neuron damage: Molecular pathways. *Handb. Clin. Neurol.* **126**, 379–399 (2014).
8. H. Kim, J. J. Kim, Y. S. Yoon, Emerging therapy for diabetic neuropathy: Cell therapy targeting vessels and nerves. *Endocr. Metab. Immune Disord. Drug Targets* **12**, 168–178 (2012).
9. A. P. Mizisin, Mechanisms of diabetic neuropathy: Schwann cells. *Handb. Clin. Neurol.* **126**, 401–428 (2014).
10. K. A. Nave, Myelination and support of axonal integrity by glia. *Nature* **468**, 244–252 (2010).
11. L. Sun *et al.*, Mixed lineage kinase domain-like protein mediates necrosis signaling downstream of RIP3 kinase. *Cell* **148**, 213–227 (2012).
12. Z. Ying *et al.*, Mixed lineage kinase domain-like protein MLKL breaks down myelin following nerve injury. *Mol. Cell* **72**, 457–468 (2018).
13. S. He *et al.*, Receptor interacting protein kinase-3 determines cellular necrotic response to TNF-α. *Cell* **137**, 1100–1111 (2009).
14. J. M. Murphy *et al.*, The pseudokinase MLKL mediates necroptosis via a molecular switch mechanism. *Immunity* **39**, 443–453 (2013).
15. B. Yan *et al.*, Discovery of a new class of highly potent necroptosis inhibitors targeting the mixed lineage kinase domain-like protein. *Chem. Commun. (Camb.)* **53**, 3637–3640 (2017).
16. W. Chen *et al.*, Diverse sequence determinants control human and mouse receptor interacting protein 3 (RIP3) and mixed lineage kinase domain-like (MLKL) interaction in necroptotic signaling. *J. Biol. Chem.* **288**, 16247–16261 (2013).
17. J. M. Murphy, The killer pseudokinase mixed lineage kinase domain-like protein (MLKL). *Cold Spring Harb. Perspect. Biol.* **12**, a036376 (2019).
18. Y. Meng *et al.*, Human RIPK3 maintains MLKL in an inactive conformation prior to cell death by necroptosis. *Nat. Commun.* **12**, 6783 (2021).
19. E. L. Feldman, K. A. Nave, T. S. Jensen, D. L. H. Bennett, New horizons in diabetic neuropathy: Mechanisms, bioenergetics, and pain. *Neuron* **93**, 1296–1313 (2017).
20. A. Viader *et al.*, Aberrant Schwann cell lipid metabolism linked to mitochondrial deficits leads to axon degeneration and neuropathy. *Neuron* **77**, 886–898 (2013).
21. T. Gordon, The role of neurotrophic factors in nerve regeneration. *Neurosurg. Focus* **26**, E3 (2009).
22. B. Beirowski *et al.*, Metabolic regulator LKB1 is crucial for Schwann cell-mediated axon maintenance. *Nat. Neurosci.* **17**, 1351–1361 (2014).
23. M. K. Jha, B. M. Morrison, Lactate transporters mediate glia-neuron metabolic crosstalk in homeostasis and disease. *Front. Cell. Neurosci.* **14**, 589582 (2020).
24. E. Domènech-Estévez *et al.*, Distribution of monocarboxylate transporters in the peripheral nervous system suggests putative roles in lactate shuttling and myelination. *J. Neurosci.* **35**, 4151–4156 (2015).
25. S. Kiryu-Seo, N. Ohno, G. J. Kidd, H. Komuro, B. D. Trapp, Demyelination increases axonal stationary mitochondrial size and the speed of axonal mitochondrial transport. *J. Neurosci.* **30**, 6658–6666 (2010).
26. S. Pan, J. R. Chan, Regulation and dysregulation of axon infrastructure by myelinating glia. *J. Cell Biol.* **216**, 3903–3916 (2017).
27. H. Wang *et al.*, Mixed lineage kinase domain-like protein MLKL causes necrotic membrane disruption upon phosphorylation by RIP3. *Mol. Cell* **54**, 133–146 (2014).
28. A. L. Samson *et al.*, A toolbox for imaging RIPK1, RIPK3, and MLKL in mouse and human cells. *Cell Death Differ.* **28**, 2126–2144 (2021).
29. D. Li *et al.*, RIPK1-RIPK3-MLKL-dependent necrosis promotes the aging of mouse male reproductive system. *eLife* **6**, e27692 (2017).
30. B. L. Furman, Streptozotocin-induced diabetic models in mice and rats. *Curr. Protoc. Pharmacol.* **70**, 5.47.1–5.47.20 (2015).
31. M. J. Stevens, I. Obrosova, X. Cao, C. Van Huysen, D. A. Greene, Effects of DL-α-lipoic acid on peripheral nerve conduction, blood flow, energy metabolism, and oxidative stress in experimental diabetic neuropathy. *Diabetes* **49**, 1006–1015 (2000).

Downloaded from https://www.pnas.org by 217.105.28.28 on April 14, 2025 from IP address 217.105.28.28.